2019

Fabrication and In-Situ Cross-linking of Carboxylic Acid-Functionalized Poly(ester amide) Scaffolds for Tissue Engineering

Kai Cao
Western University, kaicao91@gmail.com

Derek S. Flegg
Western University, dflegg@uwo.ca

Shigang Lin
Western University

Francois Lagugne-Labarthet
Western University

Kibret Mequanint
Western University

See next page for additional authors

Fabrication and *In-Situ* Cross-linking of Carboxylic Acid-Functionalized Poly(ester amide) Scaffolds for Tissue Engineering

Kai Cao,[a] Derek S. Flegg,[b] Shigang Lin,[b] François Lagugné-Labarthet,[a] Kibret Mequanint,[b] and Elizabeth R. Gillies[a,b*]

[a]Department of Chemistry and the Centre for Advanced Materials and Biomaterials Research, The University of Western Ontario, 1151 Richmond St., London, Ontario, Canada, N6A 5B7

[b]Department of Chemical and Biochemical Engineering, The University of Western Ontario, 1151 Richmond St., London, Ontario, Canada, N6A 5B9

*author to whom correspondence should be addressed: egillie@uwo.ca

Abstract

Three-dimensional (3D) scaffolds are important tools for tissue engineering, and should ideally provide both biochemical cues and biomechanical support for cells. Poly(ester amide)s (PEAs) have emerged as promising materials for the preparation of tissue engineering scaffolds and the pendant side chains of residues such as L-lysine and L-aspartic acid can provide sites for the conjugation of biochemical signals. However, it has been challenging to combine scaffold morphological stability with the presentation of reactive groups on PEA scaffolds. We describe here a new approach involving the functionalization of a L-lysine-containing PEA with maleic anhydride to simultaneously introduce cross-linkable alkenes and carboxylic acid conjugation sites. Maleic-acid-functionalized PEA was processed to form 3D scaffolds using a salt leaching method and the scaffolds were cross-linked *in situ* using a poly(ethylene glycol) dimethacrylate cross-linking agent by thermal free radical curing. Micro-computed tomography analysis indicated

that the cross-linked scaffolds had higher polymer volume fraction, lower porosity, and smaller pore size than the non-cross-linked scaffolds, but both scaffolds exhibited high morphological stability and negligible mass loss upon incubation in phosphate buffered saline for 5 days. The Young's moduli of the cross-linked and non-cross-linked scaffolds were 28 and 9 kPa respectively. Fluorescein-labeled bovine serum albumin was successfully conjugated to the scaffolds using a carbodiimide-based coupling. Finally, it was shown that the scaffolds supported the attachment and proliferation of mouse embryonic mesenchymal multipotent cells, showing their promise as platforms for tissue engineering applications.

Keywords

Poly(ester amide), tissue engineering, protein conjugation, cross-linking, scaffold

Introduction

Tissue engineering involves the use of a combination of cells, scaffolds, and appropriate biochemical and physicochemical factors to replace or improve biological tissues.[1-2] Scaffold design and fabrication play critical roles in the process of engineering tissues as the ideal scaffold should mimic both mechanically and functionally the properties of the tissues being regenerated.[3-5] Biopolymers such as gelatin,[6-7] hyaluronic acid,[8] cellulose,[9] and collagen[10] as well as decellularized tissues[11] have been used to prepare tissue engineering scaffolds with the advantage of retaining the biochemical and biomechanical properties of the native extracellular matrix (ECM). However, they exhibit limited ability to be chemically and mechanically tuned. Many synthetic polymers including polyurethane,[12] poly(lactic acid),[4] poly(ε-caprolactone)[13] have also been investigated for scaffold preparation. While often lacking the resemblance to the native ECM, the mechanical properties, degradation rates and the porosities of scaffolds prepared from synthetic

polymers can be easily tailored.[14] In addition, synthetic polymers can be reproducibly prepared and purified on a large scale, and different functional groups can be introduced to the scaffold for post-modification.[15]

Poly(ester amide)s (PEAs) have been emerging as a promising class of synthetic polymers for the preparation of tissue engineering scaffolds.[16-22] The combination of both amide and ester linkages in PEA backbones imparts excellent thermal and mechanical properties like polyamides as well as the biodegradability of polyesters.[23] In addition, amino acid-containing PEAs can benefit from the pendant functionalities on the amino acid side chains.[17, 24-26] Amino acid-containing PEAs were shown to support the growth of bovine aortic endothelial cells[27-28] and human coronary artery smooth muscle cells[29] when incorporated into hydrogels or electrospun 3D scaffolds respectively. In addition, they were shown to exhibit high blood and cytocompatibility as well as the ability to prevent the corrosion of magnesium substrates, properties that are important for potential biomedical device coating applications.[30-32] PEA scaffolds have also been used to encapsulate and release bioactive molecules such as nitroxyl radicals,[33] bactericides,[18] fibroblast growth factor-9,[34] and cell priming factors.[35] We have focused on the synthesis of PEAs having reactive pendant groups[36-38] to which bioactive molecules such as growth factors can be conjugated. For example, PEAs containing aspartic acid were used to fabricate 3D scaffolds by electrospinning and transforming growing factor-β1 was conjugated to the pendant acid groups.[29] However, the scaffolds suffered from poor morphological stability, and fiber fusion was observed upon immersion in buffer.

To preserve the 3D morphology of polymeric scaffolds, cross-linking has been used.[39-40] In contrast with the intensive exploration of post scaffold fabrication methods,[41-42] *in situ* scaffold fabrication and cross-linking, has rarely been reported. However, taking advantage of the UV-light-

triggered thiol-ene reaction, a few examples of UV cross-linked fibers were reported recently.[43-45] We report here a new L-lysine-containing PEA with maleic acid grafted to the pendant ε-amines of the lysine residues. The maleic acid simultaneously provides double bonds that enable thermal cross-linking of the polymer, while its carboxylic acid provides a conjugation site. The preparation and cross-linking of scaffolds using a salt leaching method is described, followed by their physicochemical and mechanical characterization. Conjugation of a protein to the scaffolds is described and the evaluation of cytocompatibility with mouse embryonic mesenchymal multipotent cells is also explored. To the best of our knowledge, this work constitutes the first example of a 3D porous PEA scaffold with pendant reactive groups.

Experimental

General materials. BOC-Lys-PEA composed of sebacic acid and the bis(α-amino acid) α,ω-alkylene diesters prepared from 1,4-butanediol and either L-phenylalanine (Phe) or ε-*t*-butyloxycarbonyl (BOC)-protected L-lysine (Lys) (80:20 Phe:Lys monomers) was prepared as previously reported.[37] The number average molar mass (M_n) was 31,300 g/mol and the dispersity (*Đ*) was 2.64 (Figures S1). Poly(ethylene glycol) dimethylacrylate 2000 g/mol (PEG-DMA)[46] and fluorescein isothiocyanate-functionalized bovine serum albumin (FITC-BSA)[47-48] were synthesized according to the previously reported procedures. All reactions were carried out under a N_2 (g) atmosphere unless otherwise stated. Maleic anhydride was purchased from Alfa Aesar and recrystallized from $CHCl_3$ before use. Azobisisobutyronitrile (AIBN), BSA, and *N*-(3-dimethylaminopropyl)-*N'*ethylcarbodiimide (EDC) were purchased from Sigma-Aldrich and used as received. FITC and *N*-hydroxysulfosuccinimide sodium salt (sulfo-NHS) were purchased from Alfa Aesar. CH_2Cl_2, trifluoroacetic acid (TFA), NEt_3, pyridine, *N*,*N*-dimethylformamide (DMF), and diethyl ether were purchased from Caledon Laboratories and used as received unless otherwise

indicated. NEt_3 was freshly distilled over CaH_2 under N_2 (g). DMF and CH_2Cl_2 were dried using a solvent purification system based on aluminum oxide columns.

General procedures. Fourier transform infrared (FT-IR) spectra were obtained using a PerkinElmer FT-IR Spectrum Two instrument in attenuated total reflectance (ATR) mode. ^{1}H NMR spectra were obtained on 400 MHz or 600 MHz Varian Inova instruments. NMR chemical shifts (δ) were calibrated against the residual solvent signal of DMSO-d_6 (2.5 ppm) and are expressed in parts per million (ppm). Coupling constants (J) are given in Hz. Size exclusion chromatography (SEC) was performed using a Waters 515 HPLC pump equipped with a Waters In-Line Degasser AF, two PLgel mixed D 5 µm (300 × 1.5 mm) columns connected to a corresponding PLgel guard column, and a Wyatt Optilab rEX refractive index detector operating at 658 nm. Samples were dissolved in DMF containing 10 mM LiBr and 1% v/v NEt_3 at a concentration of ~5 mg/mL. Each sample was filtered through a 0.22 µm PTFE syringe filter prior to injection using a 50 µL loop. Samples were run at a flow rate of 1 mL/min for 30 min at 85 ºC. Molar masses of the samples were calculated relative to poly(methyl methacrylate) standards. Thermogravimetric analysis (TGA) was performed on a TA Q50 instrument with a heating rate of 10 ºC/min up to a maximum temperature of 1000 ºC under N_2 (g). Differential scanning calorimetry (DSC) thermograms were obtained using a TA Q2000 instrument with a heating/cooling rate of 10 ºC/min between -60 and 120 ºC under N_2 (g). The melting temperature (T_m) and midpoint glass transition temperature (T_g) were obtained from the second heating cycle.

Preparation of TFA·H_3N-Lys-PEA. BOC-Lys-PEA (2.3 g) was dissolved in 10 mL of dry CH_2Cl_2, then 10 mL of TFA were added. The solution was stirred at room temperature for 2 h. Afterwards, CH_2Cl_2 and TFA were removed by evaporation under N_2 (g). Then, the crude product was re-dissolved in CH_2Cl_2 and precipitated into cold diethyl ether, yielding a white precipitate.

The precipitate was collected *via* filtration and dried under vacuum overnight. Yield: 1.4 g, 61 %. After confirmation of BOC group removal by ^{1}H NMR spectroscopy (Figure S3), the product was immediately taken to the next step.

Synthesis of maleic acid-PEA. TFA·H_3N-Lys-PEA (1.4 g, 0.80 mmol of amine, 1.0 equiv) was dissolved in dry DMF (10 mL) under N_2 (g). NEt_3 (2.8 mL, 20 mmol, 25 equiv) was added to the solution then it was stirred for 10 min. Pyridine (5.6 mL, 70 mmol, 87 equiv) was then added and the resulting solution was stirred for 5 min. Finally, maleic anhydride (157 mg, 1.60 mmol, 2.0 equiv) was added to the mixture and the reaction was stirred overnight at 70 °C. Afterwards, the solution was cooled to room temperature, and transferred to a regenerated cellulose dialysis membrane with molecular weight cut-off of 10,000 g/mol. The product was dialyzed against DMF for 24 h, with one change of DMF at 8 h. The DMF was then removed under vacuum, and the product was re-dissolved in CH_2Cl_2. The CH_2Cl_2 solution was precipitated into cold diethyl ether, yielding a light yellow solid. The yellow solid was collected by filtration and dried overnight under vacuum. Yield: 800 mg, 57%. ^{1}H NMR (400 MHz, DMSO-d_6): δ 9.34-9.16 (br, 0.3H, N***H***-C(O)-CH=CH-COOH), 8.23 (d, 2H, *J* = 8.2, -C(O)-N***H***-C_αH-CH_2Ph), 8.15 (d, 0.4H, *J* = 5.5, C(O)-N***H***-C_αH-$(CH_2)_4$NH-C(O)-CH=CH-COOH), 7.32-7.06 (m, 10H, ***Ph***), 6.49-6.39 (d, 0.2H, *J* = 12.7, NH-C(O)-C***H***=CH-COOH), 6.28-6.17 (d, 0.2H, *J* = 12.4, NH-C(O)-CH=C***H***-COOH), 4.53-4.35 (m, 1.8H, C_α***H***-CH_2Ph), 4.23-4.08 (br, 0.4H, C(O)-NH-C_α***H***-$(CH_2)_4$NH-C(O)-CH=CH-COOH), 4.08-3.85 (m, 4.3H, -C(O)O-C***H***$_2$-), 3.08-2.73 (m, 4H, C_αH-C***H***$_2$Ph, C_αH-CH_2-CH_2-CH_2-C***H***$_2$-NH-C(O)-CH=CH-COOH), 2.75 (br, C_αH-CH_2-CH_2-CH_2-C***H***$_2$-NH-C(O)-CH=CH-COOH), 2.21-2.07 (m, 0.8H, C_αH-C***H***$_2$-CH_2-CH_2-CH_2-NH-C(O)-CH=CH-COOH), 2.03 (t, 4H, *J* = 7.0, NHCO-C***H***$_2$-CH_2-CH_2-CH_2-CH_2-CH_2-CH_2-C***H***$_2$-CONH), 1.60 (br, 1H, C_αH-CH_2-CH_2-C***H***$_2$-CH_2-NH-C(O)-CH=CH-COOH), 1.53-1.28 (m, 9H, -C(O)-O-CH_2-C***H***$_2$-, NHCO-CH_2-C***H***$_2$-CH_2-CH_2-CH_2-CH_2-

C***H***$_2$-CH$_2$-CONH, C$_\alpha$H-CH$_2$-C***H***$_2$-CH$_2$-CH$_2$-NH-C(O)-CH=CH-COOH), 1.28-1.0 (m, 10H, NHCO-CH$_2$-CH$_2$-C***H***$_2$-C***H***$_2$-C***H***$_2$-C***H***$_2$-CH$_2$-CH$_2$-CONH). FT-IR (cm^{-1}): 3305 (N-H, stretch, amide), 3065 (C-H stretch, aromatic), 3031 (C-H stretch, aromatic), 2925 (C-H stretch, aliphatic), 2857 (C-H stretch, aliphatic), 1736 (C=O stretch, ester), 1649 (C=O stretch, amide I), 1537 (N-H bend, C-N stretch, amide II), 1498 (C=C stretch, aromatic), 1455 (CH$_2$ wag, aliphatic), 1180 (C-O stretch, ester), (CH=CH out of plane bend) SEC: M_n = 20,100 g/mol, M_w = 49,400 g/mol, $Đ$ = 2.46.

Gel content determination. Maleic acid-PEA (100 mg) was dissolved in 0.40 mL of DMF in a Schlenk flask. To this solution, PEG-DMA (25 mg, 25 wt% relative to maleic acid-PEA) and AIBN (9 mg) were added. The mixture was degassed by three freeze-pump-thaw cycles and sealed in under N_2. The sealed flask was heated at 75 °C for 48 h. Afterwards, the flask was cooled to room temperature and the product was washed vigorously with DMF using a vortex mixer for 15 min, and the yellow supernatant was discarded. The washing process was repeated three times to ensure the unreacted maleic acid-PEA and PEG-DMA were removed. The remaining solid was then washed with acetone and dried under vacuum at room temperature overnight. The experiment was repeated in triplicate and the gel content was determined as follows:

$$Gel\ content\ (\%) = \frac{mass\ of\ the\ insoluble\ material}{mass\ of\ maleic\ acid - PEA + mass\ of\ PEG - DMA}\ \text{x}\ 100$$

Fabrication of non-cross-linked maleic acid-PEA scaffold. Ground and sieved NH_4Cl particles (180-210 μm), serving as a porogen, was packed into a cylindrical glass infiltration chamber with a diameter of 6 mm. The maleic acid-PEA in DMF (500 mg/mL, 0.4 mL) was subsequently poured over the porogen bed. The solvent was then evaporated in a fume hood for two days at room temperature. Afterwards, the scaffold was pushed out from the glass tube and the porogen NH_4Cl and any residual DMF were leached by immersing the scaffold in deionized water for 24 h at room

temperature. The scaffold was then dried in a fume hood for one day at room temperature.

Fabrication of cross-linked maleic acid-PEA scaffold. For the fabrication of the cross-linked scaffold, AIBN (18.8 mg) and PEG-DMA (50 mg) were added to the PEA-maleic acid DMF solution (500 mg/mL, 0.4 mL). Following infiltration, the porogen scaffold construct was put in a Schlenk tube and the system was gently purged with N_2 for 30 min to remove the oxygen. Then, the Schlenk tube was sealed under N_2 and heated at 75 °C for 40 h in an oven. Afterwards, the Schlenk tube was cooled to room temperature and the scaffold was pushed out from the glass tube. The porogen NH_4Cl and any residual DMF were then leached by immersing the scaffold in deionized water for 24 h at room temperature. The scaffold was then allowed to dry in a fume hood for one day at room temperature.

Scanning electron microscopy (SEM). The scaffolds were mounted on carbon taped aluminum stubs and sputtered with gold at a rate of 5 nm/min for 4 min (Hummer-6 sputtering system, Anatech, Union City, California). SEM was performed on a Hitachi S-3400N instrument at a voltage of 10 kV (Hitachi, Toyko, Japan). Images were obtained after scaffold preparation as described above. Scaffolds were then incubated in pH 7.4 phosphate buffered saline (PBS) at 37 °C for 5 days, carefully rinsed three times with deionized water, dried at room temperature in a fume hood, and imaged again.

Mass loss from maleic acid-PEA scaffolds. Scaffolds were cut into small species with diameters of 4.0 mm and thicknesses of 1.3 mm and then accurately weighed. The scaffolds were then placed into capped tubes containing 2 mL of pH 7.4 PBS and incubated at 37 °C for 5 days. The PBS was changed on day two. Afterwards, the samples were carefully rinsed three times with distilled water and subsequently lyophilized overnight. The scaffolds were re-weighed and the final mass was compared to the initial mass to calculate the mass change. The experiments were performed in

triplicate for each scaffold type.

Micro-computed tomography (micro-CT). Scaffolds were imaged using an eXplore Locus SP microCT (GE Healthcare, Canada). The samples were scanned at 20 μm voxel resolution, using an exposure time of 4500 ms, 10 frames per view, and a total of 900 views at an increment of 0.4°. Two-dimensional slice images were reassembled from the isotropic slice data, and compiled to generate a 3D image. 3D Images were analyzed and displayed using commercially available trabecular bone analysis software (MicroView version Viz+2.0, GE Healthcare). Detailed analysis of these micro-CT images includes measurements of hybrid volume fraction, porosity, pore wall thickness and pore sizes, and surface area to volume ratio.

Measurement of Young's moduli of the scaffolds. Scaffolds were cut into small slices with diameters of 4-5 mm and thicknesses of 1.4-1.6 mm using a razor blade. The exact dimensions were measured using a caliper. The scaffolds were measured in both dry and hydrated conditions. For the hydrated conditions, the scaffolds were incubated in PBS (pH = 7.4) for 2 h before measurement. All samples were measured in at least triplicate. Measurements were performed using a unconfined compression apparatus similar to that previously reported by Keller and Sottos,[49] using a 10 g load cell. Additional details on the instrument are described in the supporting information (Figures S8-S9, Table S1). Displacement was applied at a rate of 5.0 μm/s over a distance of 2.4-3.5 mm, affording a maximum load of 4-5 mN/mm^2. Young's moduli were calculated as the slopes of the linear regions of the stress-strain curves (Figure S10).

Conjugation of FITC-BSA to the maleic acid-PEA scaffold. FITC-BSA as a model protein was conjugated to the maleic acid-PEA scaffold. The scaffold (8.0 mg) was immersed in 4-morpholineethanesulfonic acid (MES) buffer (0.1 M, pH = 5.0, 4.0 mL) in a 20 mL glass vial which contained EDC (2 mM) and sulfo-NHS (5 mM) to activate the pendant carboxylic acid

groups on the scaffold. After 15 min, the MES buffer was removed and replaced by phosphate buffer (10 mM, pH 8.5, 4.0 mL). Then, the FITC-BSA was added to reach a final concentration of 1.5 mg/mL and was reacted for 2 h. The conjugated scaffold was then washed three times with PBS (pH 7.4) and deionized water (5 min each wash). FITC-BSA was conjugated to both non-cross-linked and cross-linked scaffolds. For the control experiments involving physical adsorption, the scaffold was subjected to the same conditions but without the addition of EDC coupling agent and sulfo-NHS.

Confocal microscopy. Scaffolds with FITC-BSA conjugated or adsorbed were imaged using a Zeiss LSM 510DUO Vario confocal microscope (Zeiss, Canada). The samples were excited at 488 nm using an Argon/2 laser with laser intensity of 17 % and the signal was captured with an LP 505 nm emission filter. The same gain (708) and digital offset (0.01) were used for the FTTC-BSA conjugated or adsorbed scaffolds.

Cell culture and DNA content assay. Mouse embryonic mesenchymal multipotent cells (10T1/2 cells) were maintained in high glucose Dulbecco's Modified Eagle's medium (DMEM, Gibco, ThermoFisher Scientific, Burlington, ON) with 5% fetal bovine serum, incubated at 37 °C and 5% CO_2. On the day of cell seeding, scaffolds were sterilized in 70% ethanol for 30 min followed by three rinses with Hank's Balanced Salt Solution (HBSS, Invitrogen, Burlington, ON), and then changed to normal culture medium for equilibration in a tissue culture hood. Cell proliferation was evaluated by quantifying the DNA content with CyQUANT® Cell Proliferation Assay kit (ThermoFisher Scientific, Burlington, ON). 3000 cells per scaffold were seeded and cultivated for 3 and 7 days. On the day of harvesting, samples were rinsed thoroughly with PBS and stored at -80 °C. Frozen samples were lysed in 200 µL of lysis buffer to release the DNA. The supernatants were collected for assay after brief centrifugation. Fluorescence intensity of DNA content was

determined fluorometrically using an excitation wavelength of 480 nm and an emission wavelength of 520 nm on a PerkinElmer 1420 Multilabel Counter. The background reading of a cell-free control was subtracted. Three independent experiments were conducted in triplicate scaffolds for each experiment. Statistical analyses were performed using student's t-test.

Fluorescence staining and confocal microscopy. Cell-seeded scaffolds at 4 and 7 days of culture were fixed in 4% (w/v) paraformaldehyde (EMD Chemicals Inc. Gibbstown, NJ) followed by permeabilization for 10 min in PBS containing 0.1% (v/v) Triton X-100. 4',6-Diamidino-2-phenylindole (DAPI; 300 nmol in PBS; Life Technologies) was used to visualize cell nuclei and F-actin was observed with Alexa^{TM} Fluor 594-conjugated phalloidin (1:100; Life Technologies). Images were taken with a Zeiss LSM 510 confocal microscope (Zeiss, Canada) equipped with an Ar/Ne as well as a UV laser.

Results and Discussion

Synthesis of maleic acid-PEA

BOC-Lys-PEA with an M_n of 31,300 g/mol with $Đ$ of 2.64 was synthesized using an interfacial polycondensation procedure as previously reported,[36, 38] and then the BOC protecting groups were removed using 1:1 TFA:CH_2Cl_2 to afford TFA·H_3N-Lys-PEA (Scheme 1). As shown in Figure 1a, a peak in the ^{1}H NMR spectrum at 7.65 ppm (labeled d) was attributed to the protons from the amine salt. Peaks at 4.17 ppm (labeled c) and 8.1 ppm (labeled b) arising from C_αH and N*H*CO adjacent to C_αH, respectively, further confirmed the presence of Lys monomer after deprotection.[38] The maleic acid modified PEA was synthesized by the reaction of TFA·H_3N-Lys-PEA with maleic anhydride in the presence of NEt_3 and pyridine. In the ^{1}H NMR spectrum, the peak at 7.65 ppm assigned to protons in the protonated amine salt of TFA·H_3N-Lys-PEA disappeared after the reaction (Figure 1b). In addition, two doublets at 6.2 and 6.4 ppm (labeled e and f) corresponding

to the alkene moieties on the maleic acid[50] were observed. Relative peak integrations suggested that at least 95% of the pendant amines on the Lys had been reacted (Figure S4).

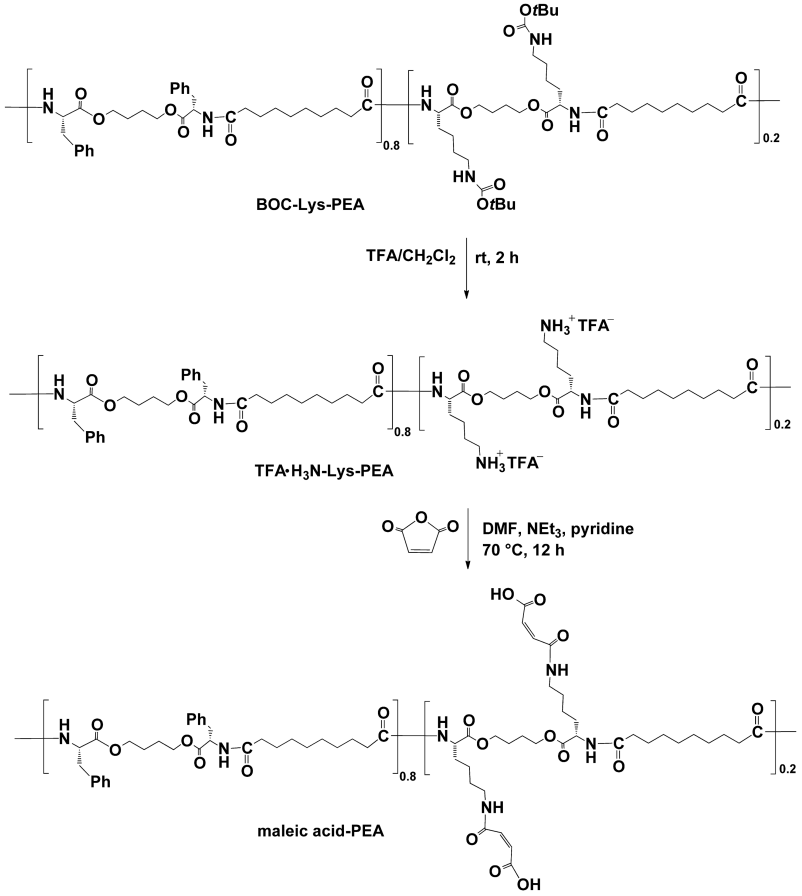

Scheme 1. Synthesis of maleic acid-PEA.

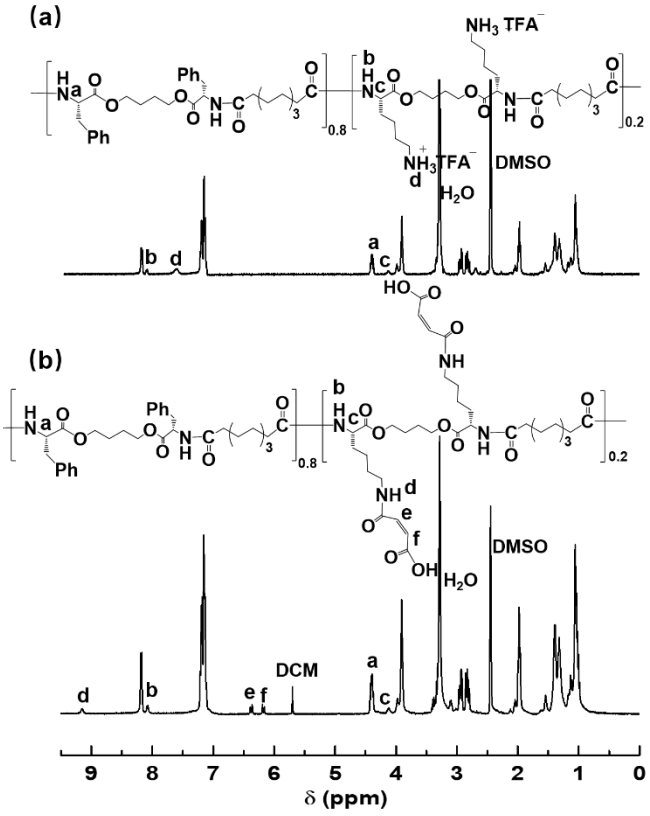

Figure 1. ^{1}H NMR spectra for (a) TFA·H_3N-Lys-PEA and (b) maleic acid-PEA (DMSO-d_6, 400 MHz) showing peaks consistent with the conversion of the protonated amines to the corresponding amides following reaction with maleic anhydride.

The chemical structure of maleic acid-PEA was further confirmed using FT-IR spectroscopy. Peaks at 1736 cm^{-1} and 1649 cm^{-1} corresponding to the ester and amide C=O stretches respectively and at 1537 cm^{-1} attributed to the N-H and C-N in the amide[38] were observed for both TFA·H_3N-Lys-PEA and maleic acid-PEA (Figure 2). The expected C=C stretching from maleic acid-PEA, which should appear at 1640 cm^{-1}, was not observed, likely due to overlap with the peak at 1649 cm^{-1}. However, analysis of the fingerprint region of the spectra showed that peaks at 833 cm^{-1}, 798 cm^{-1} and 720 cm^{-1} ascribed to the amine TFA salt[51-52] were observed for TFA·H_3N-Lys-PEA (Figure

2a) but disappeared in the spectrum of maleic acid-PEA (Figure 2b). A new broad peak at 798 cm^{-1} due to CH=CH out of plane bending and a new peak at 851 cm^{-1} corresponding to the NH from the *NH*COCH=CH out of plane bending were observed, confirming the presence of maleic acid groups in the maleic acid-PEA (Figure 2b).

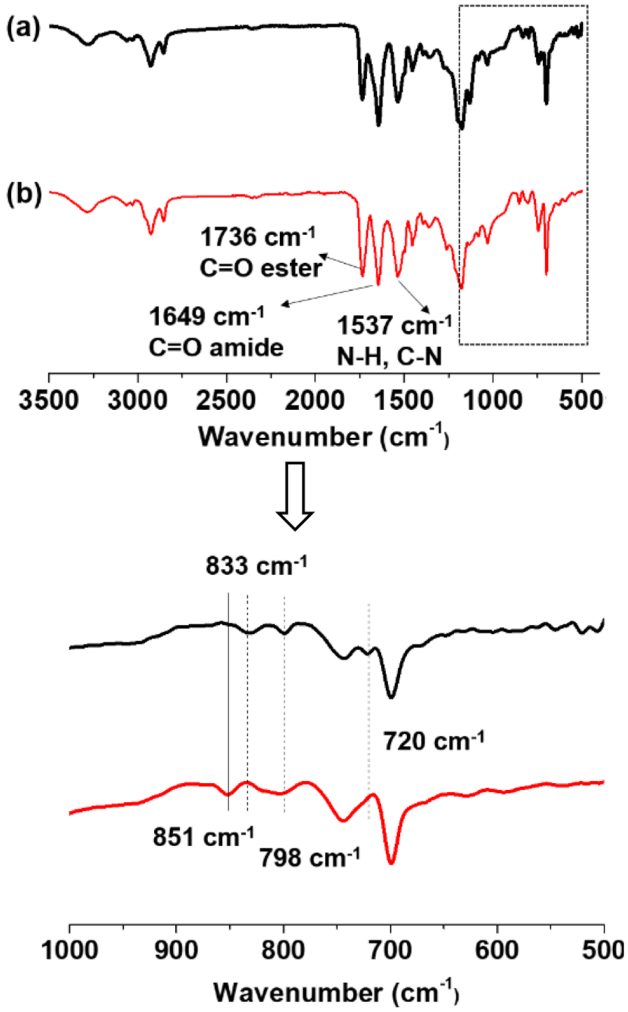

Figure 2. FT-IR spectra for (a) TFA·H_3N-Lys-PEA and (b) maleic acid-PEA. Spectra on the bottom are zoomed versions of the fingerprint regions. The dotted lines identify peaks present only for TFA·H_3N-Lys-PEA, while the solid line shows a peak only present in maleic acid-PEA.

SEC was used to measure the molar mass of maleic acid-PEA to confirm that significant degradation did not occur during the reaction sequence. Compared to BOC-Lys-PEA, maleic acid-PEA exhibited a slightly longer retention time (Figure 3), corresponding to lower M_n of 20,000 g/mol and a similar $Đ$ of 2.46. This modest reduction in M_n without an increase in $Đ$ may be caused by interactions between the carboxylic acid groups in maleic acid-PEA and column packing materials or a change in polymer hydrodynamic volume resulting from maleic acid incorporation.

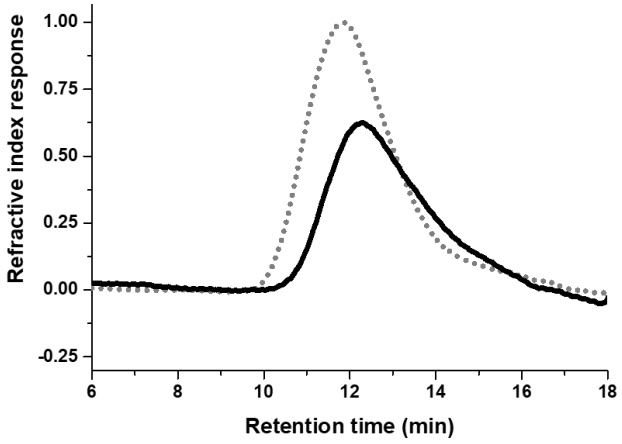

Figure 3. DMF SEC traces for BOC-Lys-PEA (grey dotted curve) and maleic acid-PEA (black solid curve) showing a minor increase in the retention time for maleic acid-PEA.

Cross-linking of maleic acid-PEA

The double bonds on the pendant maleic acid groups confer to the PEA the potential to be covalently cross-linked. The cross-linking of maleic acid-PEA (25 wt/vol%) in DMF at 75 °C in the presence of AIBN was investigated, but no gelation was observed, likely due to the low reactivity of the alkene group. However, upon the addition of 25 wt% PEG-DMA relative to maleic acid-PEA, gelation was observed and a gel content of 74 ± 6 % was obtained. To verify the occurrence of cross-linking, the gel fraction was analyzed using FT-IR spectroscopy. Characteristic peaks at 1736 cm^{-1}, 1537 cm^{-1} and 1641 cm^{-1} arising from PEA dominated the spectrum, and the

intensity of the peak at 798 cm^{-1} corresponding to the alkene on maleic acid-PEA was reduced in cross-linked maleic acid-PEA, confirming the polymerization of the alkenes into the network (Figure 4).

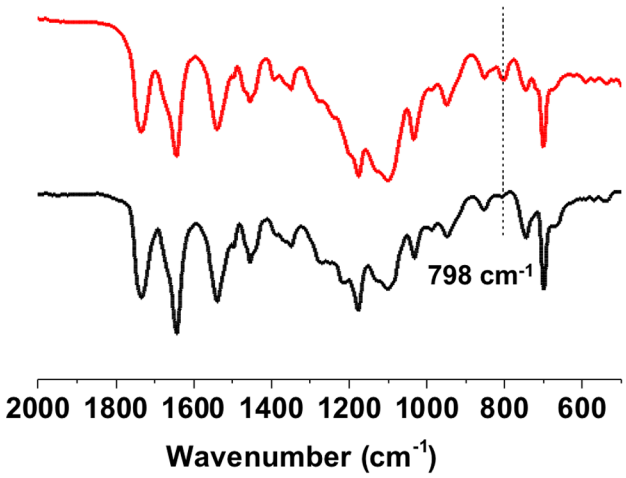

Figure 4. FT-IR spectra for maleic acid-PEA (red, top) and the cross-linked maleic acid-PEA (black, bottom), showing a reduction in the peak at 798 cm^{-1} following cross-linking (dotted line).

Scaffold fabrication and characterization

Salt leaching is a commonly used method for scaffold fabrication, as the pore size and porosity of the scaffold can be controlled by using porogens of different size and quantity.[12, 53] For the current work, NH_4Cl particles sieved to diameters of 180-210 μm were employed to achieve suitable pore sizes for cells. DMF was selected as the solvent as maleic acid-PEA was highly soluble in DMF. In addition, its high boiling point facilitated the thermally-initiated free radical cross-linking reaction. To achieve a viscous polymer solution to infiltrate the prepacked porogen bed, we selected 500 mg/mL of maleic acid-PEA as the concentration because beyond this the solution became extremely viscous and did not infiltrate. AIBN and PEG-DMA were added for the cross-linked scaffolds and the polymer-porogen construct was heated at 75 °C for 48 h before the

evaporation of the DMF. Then, the salt and any residual DMF were leached out and the scaffold was dried. For the non-cross-linked scaffolds, no heating or addition of AIBN/PEG-DMA were performed. Instead, the DMF was evaporated and the salt was leached following scaffold preparation. The first evidence of a successful cross-linking was that while the non-cross-linked scaffolds were readily dissolved in DMF, the cross-linked scaffolds were not soluble in DMF (Figure S5). Instead, the cross-linked scaffolds swelled by 17 ± 4 % relative to their initial masses.

After salt leaching, the scaffolds were examined by SEM both before and after incubation in PBS at 37 °C for 5 days. The images showed that microporous structures were formed for both cross-linked and non-cross-linked maleic-acid-PEA (Figure 5). The cross-linked and non-cross-linked scaffolds had similar morphologies prior to immersion in PBS (Figure 5a,b,e,f). After immersion in PBS, some micrometer-scale wrinkling was observed for the non-cross-linked structures, but overall the scaffolds maintained their structural integrity (Figure 5c,d,g,h). This result contrasted with our previously reported work on electrospun mats prepared from an aspartic acid-containing PEA with pendant carboxylic acid functional groups, where rapid fiber fusion was observed in PBS.[29] For the cross-linked maleic acid-PEA scaffolds, structural integrity was also preserved during immersion in PBS, though porosity at the micron and sub-micrometer level increased. This may correspond to the beginning of PEA degradation through hydrolysis, facilitated by the incorporation of hydrophilic PEG-DMA into the materials. To further probe the degradation of the scaffolds, their mass loss was measured after immersion in PBS at 37 °C for 5 days. The non-cross-linked maleic acid-PEA scaffolds underwent a mass change of +8 ± 11% while the cross-linked maleic acid-PEA scaffolds underwent a mass change of -3 ± 5%. These results were not different statistically ($p = 0.2$). Thus, there was no significant mass loss from either set of scaffolds after 5 days in PBS. This result is consistent with that of previous work where the

in vitro degradation of a scaffold based on a similar PEA (without L-lysine moieties) was found to be slow, with only 21% mass loss over 28 days.[34]

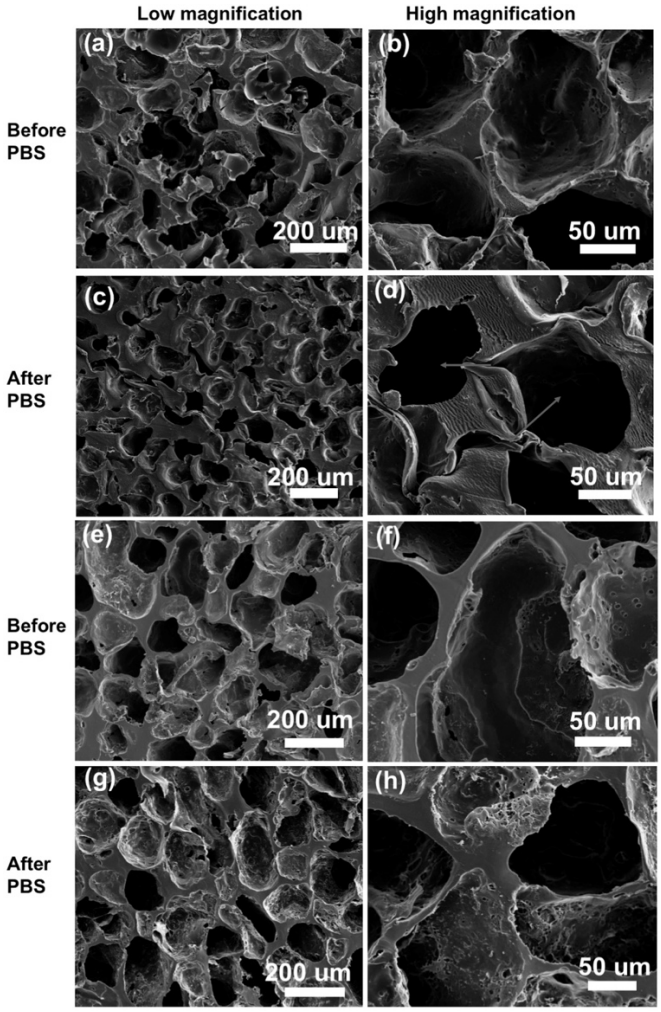

Figure 5. SEM images showing the porosity of scaffolds before and after immersion in PBS for 5 days at 37 °C: (a)-(d) non-cross-linked maleic-acid-PEA scaffolds and (e)-(h) cross-linked maleic acid-PEA scaffolds. No significant changes were observed for the non-cross-linked scaffolds, while the porosity of the cross-linked scaffolds at the micro and sub-micrometer level increased for the cross-linked scaffolds.

The scaffolds were also characterized by micro-CT. Three-dimensional models of the scaffolds

were constructed (Figure 6), enabling calculation of their bulk volume, polymer volume fraction, porosity, surface to volume ratio, pore wall thickness and pore diameter (Table 1). Both the non-cross-linked and cross-linked scaffolds had the same bulk volume (i.e., the same radius and height). The cross-linked scaffolds had a higher volume fraction of polymer and consequently lower porosity, which can be attributed to the addition of PEG-DMA to the cross-linked formulation, which results in the incorporation of more polymer into the network. The cross-linked scaffolds also had a higher surface to volume ratio, a lower pore wall thickness, and a smaller pore size, suggesting the presence of more smaller pores, compared to a smaller number of larger pores for the non-cross-linked scaffolds. A larger number of smaller pores results in a higher surface to volume ratio. While SEM images (Figure 5) indicated pore diameters similar to those of the porogens used, the pore sizes indicated by micro-CT were about 3 to 7-fold smaller. This difference can be attributed to the inclusion of micro-pores along the struts, pore walls, and the pore interconnecting windows in the micro-CT analysis.

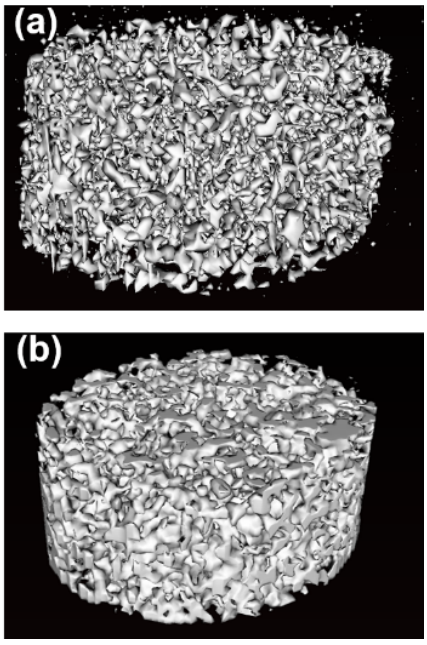

Figure 6. Micro-CT images of (a) non-cross-linked and (b) cross-linked maleic acid PEA scaffolds showing their porosity.

Table 1. Comparison of the non-cross-linked and cross-linked PEA-maleic acid scaffolds by micro-CT analysis.

Parameter	**Non-cross-linked scaffold**	**Cross-linked scaffold**
Polymer volume fraction (%)	39 ± 1	48 ± 0. 1
Porosity (%)	61.1 ± 0.9	51.9 ± 0.1
Surface area to volume ratio (mm^{-1})	60.2 ± 2.1	72.4 ± 1.2
Pore wall thickness (μm)	33.3 ± 1.2	27.7 ± 0.5
Pore size (μm)	52.6 ± 2.8	29.2 ± 0.4

The thermal properties of the scaffolds were evaluated by DSC and TGA. TGA indicated that both the non-cross-linked and cross-linked scaffolds had high thermal stability, with onset degradation temperatures of about 320 °C (Figures S6-S7). PEG-DMA was highly crystalline, with a T_m of 46 °C (Figure 7). The non-cross-linked maleic acid-PEA scaffold was amorphous with a T_g of 44 °C. The cross-linked maleic acid-PEA scaffold had a peak corresponding to a T_m of 28 °C, likely corresponding to small crystalline domains of PEG, overlaid on a broad glass transition, likely corresponding to domains of mixed PEG and PEA.

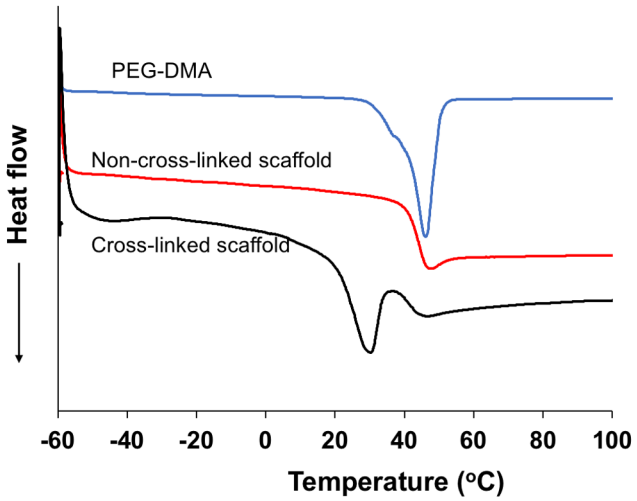

Figure 7. DSC curves for PEG-DMA (top, blue) as well as the non-cross-linked (red, middle) and cross-linked (black, bottom) maleic acid-PEA scaffolds showing that PEG-DMA is primarily crystalline, the non-cross-linked scaffold is amorphous, and the cross-linked scaffold has both crystalline and amorphous domains.

We also measured and compared the Young's moduli of the scaffolds in the dry and hydrated states. In the dry state, the non-cross-linked scaffold had a modulus of 78 kPa, compared to 41 kPa for the cross-linked scaffold (Table 2, Figure S10). The lower modulus for the cross-linked material can likely be attributed to the incorporation of PEG. The moduli of the non-cross-linked and cross-linked scaffolds in the wet state were 28 and 9 kPa respectively. Lowering of the moduli upon hydration was expected as water is known to have a significant plasticizing effect on amorphous polymers.[54] In addition, the modulus of the cross-linked scaffold decreased more in the wet state, and the PEG domains became highly hydrated. Overall, the moduli are in the range of soft organs and tissues such as the human aorta.[55]

Table 2. Young's moduli of the maleic acid-PEA scaffolds in the dry and hydrated state measured

under unconfined compression.

Scaffold	Non-cross-linked	Cross-linked
Young's modulus for dry scaffold (kPa)[a]	78 ± 13	41 ± 11
Young's modulus for hydrated scaffold (kPa)[a]	28 ± 1	9 ± 1

[a] Errors on the measurements represents the standard deviation for three different samples of scaffold.

Conjugation of FITC-BSA to the scaffolds

The purpose of incorporating pendant carboxylic acid groups into the scaffolds was to enable the conjugation of peptides and proteins that could serve as modulators of cell behavior in tissue engineering applications. Some ligands, such as those activating Notch signaling function only when immobilized.[56] Alternatively, gradual degradation of the PEA scaffold could provide a slow release of soluble ligands. It is ideal to conjugate the proteins after scaffold fabrication to avoid their denaturation during the cross-linking process. Therefore, to confirm the reactivity of the acid groups in our prepared scaffolds we conjugated FITC-BSA, a model protein with a molar mass of 69,324 g/mol. The conjugation was performed using EDC/sulfo-NHS activation of the maleic acid-PEA scaffold, followed by the addition of the protein. To demonstrate that the resulting conjugation was covalent rather than simply physical adsorption of FITC-BSA to the scaffold, a control experiment was conducted using the same conditions but without EDC/Sulfo-NHS. No fluorescence was detected in confocal microscopy for the control systems involving either cross-linked or non-cross-linked maleic acid-PEA scaffolds (Figure 8a,c), whereas covalent conjugation afforded fluorescent scaffolds with visible porous structures (Figure 8b,d). Thus, the pendant carboxylic acid groups were still reactive when incorporated into the scaffold.

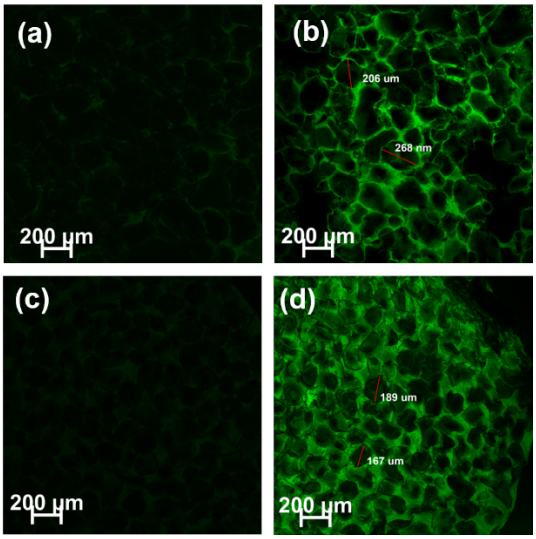

Figure 8. Fluorescence confocal microscopy images of maleic acid-PEA scaffolds following the adsorption or covalent conjugation of FITC-BSA: (a) adsorption to the non-cross-linked scaffold; (b) conjugation to the non-cross-linked scaffold; (c) adsorption to the cross-linked scaffold; (d) conjugation to the cross-linked scaffold. Only covalent conjugation afforded fluorescently labeled scaffolds.

Cell proliferation on the cross-linked PEA scaffolds

To investigate cell proliferation, attachment, and spreading on the new scaffold, we used mouse embryonic multipotent mesenchymal progenitor cell (10T1/2 cells). The rationale for using these cells is based on our prior study differentiating them towards vascular lineage for elastin-containing model tissue fabrication.[57] The cell culture work focused on the cross-linked scaffold, as the non-cross-linked scaffold was stiff and brittle, making it difficult to work with. We seeded the cells in the cross-linked maleic acid-PEA scaffold discs and cultured them for 3 and 7 days. As a control, we used a previously reported PEA composed of sebacic acid, Phe, and 1,4-butanediol, which we have already established to exhibit morphological stability as a scaffold, high cytocompatibility and to support cell proliferation.[29, 34, 38]

Cell proliferation, as indicated by the CyQUANT® DNA content assay, was significantly higher on the cross-linked scaffolds at both 3 and 7 days when compared to the controls, showing that the scaffolds were cytocompatible and supported proliferation of 10T1/2 cells (Figure 9). The cell proliferation data suggested that the cross-linking process did not introduce toxic residues to the scaffolds. Furthermore, while PEG has been found to inhibit protein adsorption and consequently protein-mediated cell adhesion,[58-59] the portion of PEG-DMA incorporated into the cross-linked scaffolds did not appear to have this effect. The robust cell proliferation was further confirmed by confocal fluorescence microscopy imaging (Figure 10). Morphologically, 10T1/2 cells were well-spread on the maleic acid-PEA scaffold with abundant F-actin expression and with cell-cell contact. Qualitatively, cells on the maleic acid-PEA scaffolds appeared to be denser and more organized as observed by well-defined F-actin fibers.

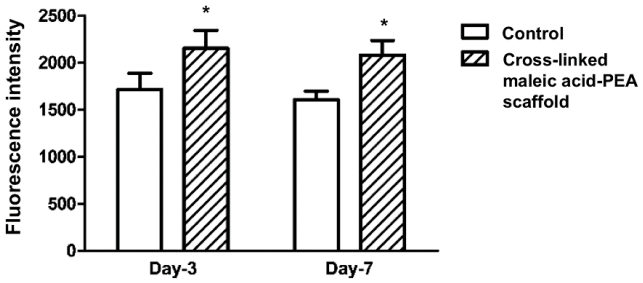

Figure 9. Fluorescence intensity measured by the CyQUANT® DNA content assay for C3H10T1/2 cells cultured for 3 and 7 days on control PEA or cross-linked maleic acid-PEA scaffolds. * indicates significantly higher cell proliferation on the cross-linked maleic acid-PEA scaffolds at both time points ($p < 0.05$, $N = 3$, $n = 3$).

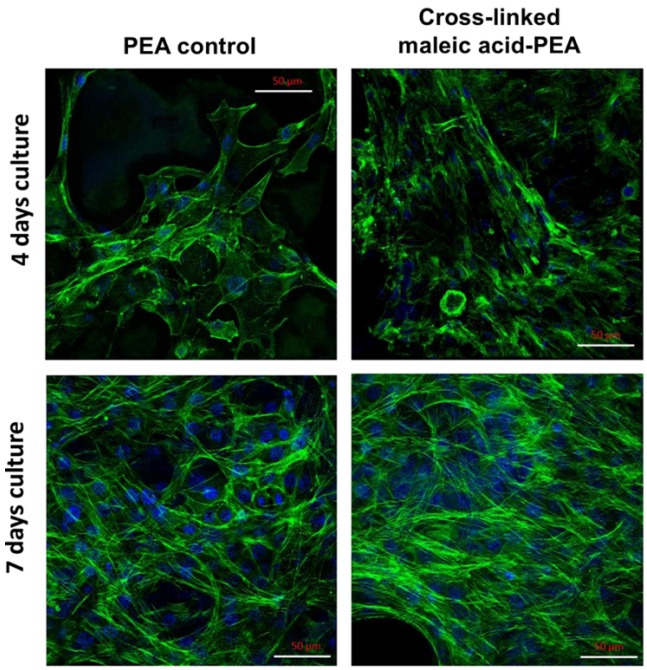

Figure 10. Fluorescence confocal microscopy images of 3D scaffold discs after culture for 4 days and 7 days with C3H10T1/2 cells, then staining of cell nuclei with DAPI (blue) and F-actin with Alexa^{TM} Fluor 594-conjugated phalloidin (green) (scale bar = 50 μm). Both the PEA control and cross-linked maleic acid-PEA scaffolds supported the adhesion of cells and increased cell densities were observed at 7 days compared to 4 days.

Conclusions

A maleic acid-functionalized PEA was successfully synthesized, providing both pendant alkenes and carboxylic acids on the polymer. It was possible to use the polymer to fabricate three-dimensional scaffolds using a salt leaching approach, and to cross-link the alkenes in the scaffolds through a thermal free radical curing approach, stabilizing their structure and altering their mechanical properties. It was also demonstrated that the carboxylic acids on the resulting scaffolds could be used to covalently immobilize proteins. The cross-linked scaffolds supported the adhesion, spreading, and proliferation of mouse embryonic multipotent mesenchymal progenitor

cells. Overall, the new scaffold represents a promising platform for three-dimensional cell culture. Through the conjugation of specific biomolecules such as growth factors it should be possible to use the platform to control and modulate the behavior of cells for a diverse range of tissue engineering applications.

Supporting information

Additional SEC and ^{1}H NMR data, scaffold swelling/dissolution, TGA data, details and data for mechanical testing

Acknowledgements

We thank the Natural Sciences and Engineering Research Council of Canada (Discovery Grant 2016-04636) for funding this work.

References

(1) van Blitterswijk, C. A.; de Boer, J., *Tissue Engineering,* 2nd ed.; Academic Press: London, UK, 2014.

(2) Mathew, A. P.; Augustine, R.; Kalarikkal, N.; Thomas, S., Tissue Engineering: Principles, Recent Trends and the Future. In *Nanomedicine and Tissue Engineering, State of the Art and Recent Trends*; Kalarikkal, N.; Augustine, R.; Oluwafemi, O. S.; Joshy, K. S.; Thomas, S., Eds.; Apple Academic Press, Inc.: Oakville, ON, Canada, 2016; pp 31-82.

(3) Khorshidi, S.; Solouk, A.; Mirzadeh, H.; Mazinani, S.; Lagaron, J. M.; Sharifi, S.; Ramakrishna, S. A Review of Key Challenges of Electrospun Scaffolds for Tissue-Engineering Applications. *J. Tissue Eng. Regen. Med.* **2016**, *10*, 715-738.

(4) Santoro, M.; Shah, S. R.; Walker, J. L.; Mikos, A. G. Poly(lactic acid) Nanofibrous Scaffolds for Tissue Engineering. *Adv. Drug Delivery Rev.* **2016**, *107*, 206-212.

(5) Webber, M. J.; Khan, O. F.; Sydlik, S. A.; Tang, B. C.; Langer, R. A Perspective on the Clinical Translation of Scaffolds for Tissue Engineering. *Annals Biomed. Eng.* **2015**, *43*, 641-656.

(6) Wu, S.-C.; Chang, W.-H.; Dong, G.-C.; Chen, K.-Y.; Chen, Y.-S.; Yao, C.-H. Cell Adhesion and Proliferation Enhancement by Gelatin Nanofiber Scaffolds. *J. Bioact. Compat. Polym.* **2011**, *26*, 565-577.

(7) Guarino, V.; Alvarez-Perez, M.; Cirillo, V.; Ambrosio, L. HMSC Interaction with PCL and PCL/Gelatin Platforms: A Comparative Study on Films and Electrospun Membranes. *J. Bioact. Compat. Polym.* **2011**, *26*, 144-160.

(8) Khunmanee, S.; Jeong, Y.; Park, H. Crosslinking Method of Hyaluronic-Based Hydrogel for Biomedical Applications. *J. Tissue Eng.* **2017**, *8*, 1-16.

(9) Gopi, S.; Balakrishnan, P.; Chandradhara, D.; Poovathankandy, D.; Thomas, S. General Scenarios of Cellulose and Its Use in the Biomedical Field. *Mater. Today Chem.* **2019**, *13*, 59-78.

(10) Dong, C.; Lv, Y. Application of Collagen Scaffold in Tissue Engineering: Recent Advances and New Perspectives. *Polymers* **2016**, *8*, https://doi.org/10.3390/polym8020042.

(11) Robb, K. P.; Shridhar, A.; Flynn, L. E. Decellularized Matrices as Cell-Instructive Scaffolds to Guide Tissue-Specific Regeneration. *ACS Biomaterials Sci. Eng.* **2018**, *4*, 3627-3643.

(12) Janik, H.; Marzec, M. A Review: Fabrication of Porous Polyurethane Scaffolds. *Mater. Sci. Eng., C* **2015**, *48*, 586-591.

(13) Cipitria, A.; Skelton, A.; Dargaville, T. R.; Dalton, P. D.; Hutmacher, D. W. Design, Fabrication and Characterization of PCL Electrospun Scaffolds—A Review. *J. Mater. Chem.* **2011**, *21*, 9419-9453.

(14) Place, E. S.; George, J. H.; Williams, C. K.; Stevens, M. M. Synthetic Polymer Scaffolds for Tissue Engineering. *Chem. Soc. Rev.* **2009**, *38*, 1139-1151.

(15) Gunatillake, P. A.; Adhikari, R. Biodegradable Synthetic Polymers for Tissue Engineering. *Eur. Cells Mater.* **2003**, *5*, 1-16.

(16) Ghosal, K.; Latha, M. S.; Thomas, S. Poly(ester amides) (PEAs) – Scaffold for Tissue Engineering Applications. *Eur. Polym. J.* **2014**, *60*, 58-68.

(17) Fonseca, A. C.; Gil, M. H.; Simoes, P. N. Biodegradable Poly(ester amide)s - A Remarkable Opportunity for the Biomedical Area: Review on the Synthesis, Characterization and Applications. *Prog. Polym. Sci.* **2014**, *39*, 1291-1311.

(18) Murase, S. K.; del Valle, L. J.; Kobauri, S.; Katsarava, R.; Puiggalí, J. Electrospun Fibrous Mats from a L-Phenylalanine Based Poly(ester amide): Drug Delivery and Accelerated Degradation by Loading Enzymes. *Polym. Deg. Stabil.* **2015**, *119*, 275-287.

(19) Murase, S. K.; Puiggalí, J., Poly(ester amide)s: Recent Developments on Synthesis and Applications. In *Natural and Synthetic Biomedical Polymers*; Kumbar, S.; Laurencin, C.; Deng, M., Eds.; Elsevier: Burlington, MA, 2014; pp 145-166.

(20) Rodriguez-Galan, A.; Franco, L.; Puiggalí, J. Degradable Poly(ester amide)s for Biomedical Applications. *Polymer* **2011**, *3*, 65-99.

(21) Díaz, A.; Katsarava, R.; Puiggalí, J. Synthesis, Properties and Applications of Biodegradable Polymers Derived from Diols and Dicarboxylic Acids: From Polyesters to Poly(ester amide)s. *Int. J. Mol. Sci.* **2014**, *15*, 7064-7123.

(22) Zavradashvili, N.; Jokhadze, G.; Gverdtsiteli, M.; Tugushi, D.; Katsarava, R. Biodegradable Functional Polymers Composed of Naturally Occurring Amino Acids. *Res. Rev. Polym.* **2017**, *8*, 105-128.

(23) Upton, B. M.; Kasko, A. M. Biodegradable Aromatic–Aliphatic Poly(ester–amides) from Monolignol-Based Ester Dimers. *ACS Sustainable Chem. Eng.* **2018**, *6*, 3659-3668.

(24) Deng, M.; Wu, J.; Reinhart-King, C. A.; Chu, C. C. Synthesis and Characterization of Biodegradable Poly(ester amide)s with Pendant Amine Functional Groups and in Vitro Cellular Response. *Biomacromolecules* **2009**, *10*, 3037-3047.

(25) Winnacker, M.; Rieger, B. Poly(ester amide)s: Recent Insights into Synthesis, Stability and Biomedical Applications. *Polym. Chem.* **2016**, *7*, 7039-7046.

(26) Ji, Y.; Li, J.; Zhao, J.; Shan, S.; Chu, C.-C. A Light-Facilitated Drug Delivery System from a Pseudo-Protein/Hyaluronic Acid Nanocomplex with Improved Anti-Tumor Effects. *Nanoscale* **2019**, *11*, 9987-10003.

(27) Wu, J.; Wu, D.; Mutschler, A.; Chu, C.-C. Cationic Hybrid Hydrogels from Amino-Acid-Based Poly(ester amide): Fabrication, Characterization, and Biological Properties. *Adv. Funct. Mater.* **2012**, *22*, 3815-3823.

(28) Pang, X.; Wu, J.; Chu, C. C.; Chen, X. Development of an Arginine-Based Cationic Hydrogel Platform: Synthesis, Characterization and Biomedical Applications. *Acta Biomater.* **2014**, *10*, 3098-3107.

(29) Knight, D. K.; Gillies, E. R.; Mequanint, K. Biomimetic L-Aspartic Acid-Derived Functional Poly(ester amide)s for Vascular Tissue Engineering. *Acta Biomater.* **2014**, *10*, 3484-3496.

(30) Lee, S. H.; Szinai, I.; Carpenter, K.; Katsarava, R.; Jokhadze, G.; Chu, C. C.; Huang, Y.;

Verbeken, E.; Bramwel, O.; De Scheerder, I.; Hong, M. K. In Vivo Biocompatibility Evaluation of Stents Coated with a New Biodegradable Elastomeric and Functional Polymer. *Coronary Artery Dis.* **2002**, *13*, 237-241.

(31) DeFife, K. M.; Grako, K.; Cruz-Aranda, G.; Price, S.; Chantung, R.; MacPherson, K.; Khoshabeh, R.; Gopalan, S.; Turnell, A. G. Poly(ester amide) Copolymers Promote Blood and Tissue Compatibility. *J. Biomater. Sci. Polym. Ed.* **2009**, *20*, 1495-1511.

(32) Liu, J.; Liu, X. L.; Xi, T. F.; Chu, C. C. A Novel Pseudo-Protein-Based Biodegradable Coating for Magnesium Substrates: In Vitro Corrosion Phenomena and Cytocompatibility. *J. Mater. Chem. B* **2015**, *3*, 878-893.

(33) Li, L.; Chu, C. C. Nitroxyl Radical Incorporated Electrospun Biodegradable Poly(ester amide) Nanofiber Membranes. *J. Biomater. Sci., Polym. Ed.* **2009**, *20*, 341-361.

(34) Said, S. S.; Pickering, J. G.; Mequanint, K. Controlled Delivery of Fibroblast Growth Factor-9 from Biodegradable Poly(ester amide) Fibers for Building Functional Neovasculature. *Pharm. Res.* **2014**, 1-13.

(35) Memanishvili, T.; Kupatadze, N.; Tugushi, D.; Katsarava, R.; Wattananit, S.; Hara, N.; Tomero, D.; Kokaia, Z. Generation of Cortical Neurons from Human Induced-Pluripotent Stem Cells by Biodegradable Polymeric Microspheres Loaded with Priming Factors. *Biomed. Mater.* **2016**, *11*, 025011.

(36) Atkins Katelyn, M.; Lopez, D.; Knight Darryl, K.; Mequanint, K.; Gillies Elizabeth, R. A Versatile Approach for the Syntheses of Poly(ester amide)s with Pendant Functional Groups. *J. Polym. Sci., Part A: Polym. Chem.* **2009**, *47*, 3757-3772.

(37) DeWit, M. A.; Wang, Z.; Atkins, K. M.; Mequanint, K.; Gillies, E. R. Syntheses, Characterization, and Functionalization of Poly(ester amide)a with Pendant Amine

Functional Groups. *J. Polym. Sci., Part A: Polym. Chem.* **2008**, *46*, 6376-6392.

(38) Knight, D. K.; Gillies, E. R.; Mequanint, K. Strategies in Functional Poly(ester amide) Syntheses to Study Human Coronary Artery Smooth Muscle Cell Interactions. *Biomacromolecules* **2011**, *12*, 2475-2487.

(39) Scott, A. S.; Michael, P. F.; Koyal, G.; Michael, J. M.; David, G. S.; Gary, L. B. Cross-Linking Methods of Electrospun Fibrinogen Scaffolds for Tissue Engineering Applications. *Biomed. Mater.* **2008**, *3*, 045001.

(40) Rowland, C. R.; Lennon, D. P.; Caplan, A. I.; Guilak, F. The Effects of Crosslinking of Scaffolds Engineered from Cartilage ECM on the Chondrogenic Differentiation of MSCs. *Biomaterials* **2013**, *34*, 5802-5812.

(41) Jordan, A. M.; Viswanath, V.; Kim, S.-E.; Pokorski, J. K.; Korley, L. T. J. Processing and Surface Modification of Polymer Nanofibers for Biological Scaffolds: A Review. *J. Mater. Chem. B* **2016**, *4*, 5958-5974.

(42) Kalaoglu-Altan, O. I.; Sanyal, R.; Sanyal, A. Reactive and 'Clickable' Electrospun Polymeric Nanofibers. *Polym. Chem.* **2015**, *6*, 3372-3381.

(43) de Oliveira, F. C. S.; Olvera, D.; Sawkins, M. J.; Cryan, S.-A.; Kimmins, S. D.; da Silva, T. E.; Kelly, D. J.; Duffy, G. P.; Kearney, C.; Heise, A. Direct UV-Triggered Thiol–Ene Cross-Linking of Electrospun Polyester Fibers from Unsaturated Poly(macrolactone)s and Their Drug Loading by Solvent Swelling. *Biomacromolecules* **2017**, *18*, 4292-4298.

(44) Kalaoglu-Altan, O. I.; Verbraeken, B.; Lava, K.; Gevrek, T. N.; Sanyal, R.; Dargaville, T.; De Clerck, K.; Hoogenboom, R.; Sanyal, A. Multireactive Poly(2-oxazoline) Nanofibers through Electrospinning with Crosslinking on the Fly. *ACS Macro Letters* **2016**, *5*, 676-681.

(45) Shanmuganathan, K.; Elliot, S. M.; Lane, A. P.; Ellison, C. J. Highly Stretchable Thermoset Fibers and Nonwovens Using Thiol–Ene Photopolymerization. *ACS Appl. Mater. Interfaces* **2014**, *6*, 14259-14265.

(46) Lin-Gibson, S.; Bencherif, S.; Cooper, J. A.; Wetzel, S. J.; Antonucci, J. M.; Vogel, B. M.; Horkay, F.; Washburn, N. R. Synthesis and Characterization of PEG Dimethacrylates and Their Hydrogels. *Biomacromolecules* **2004**, *5*, 1280-1287.

(47) Wang, C.; Ouyang, J.; Ye, D.-K.; Xu, J.-J.; Chen, H.-Y.; Xia, X.-H. Rapid Protein Concentration, Efficient Fluorescence Labeling and Purification on a Micro/Nanofluidics Chip. *Lab Chip* **2012**, *12*, 2664-2671.

(48) McDonagh, P. F.; Williams, S. K. The Preparation and Use of Fluorescent-Protein Conjugates for Microvascular Research. *Microvasc. Res.* **1984**, *27*, 14-27.

(49) Keller, M. W.; Sottos, N. R. Mechanical Properties of Microcapsules Used in a Self-Healing Polymer. *Exp. Mech.* **2006**, *46*, 725-733.

(50) Kalgutkar, A. S.; Crews, B. C.; Marnett, L. J. Design, Synthesis, and Biochemical Evaluation of N-Substituted Maleimides as Inhibitors of Prostaglandin Endoperoxide Synthases. *J. Med. Chem.* **1996**, *39*, 1692-1703.

(51) Sangsanoh, P.; Supaphol, P. Stability Improvement of Electrospun Chitosan Nanofibrous Membranes in Neutral or Weak Basic Aqueous Solutions. *Biomacromolecules* **2006**, *7*, 2710-2714.

(52) Chen, J.-P.; Chen, S.-H.; Lai, G.-J. Preparation and Characterization of Biomimetic Silk Fibroin/Chitosan Composite Nanofibers by Electrospinning for Osteoblasts Culture. *Nanoscale Res. Lett.* **2012**, *7*, 170.

(53) Mi, H.-Y.; Jing, X.; Turng, L.-S. Fabrication of Porous Synthetic Polymer Scaffolds for

Tissue Engineering. *J. Cell. Plast.* **2014**, *51*, 165-196.

(54) Hancock, B. C.; Zografi, G. The Relationship between the Glass Transition Temperature and the Water Content of Amorphous Pharmaceutical Solids. *Pharm. Res.* **1994**, *11*, 471-477.

(55) Akhtar, R.; Sherratt, M. J.; Cruickshank, J. K.; Derby, B. Characterizing the Elastic Properties of Tissues. *Mater. Today* **2011**, *14*, 96-105.

(56) Tiemeijer, L. A.; Frimat, J.-P.; Stassen, O. M. J. A.; Bouten, C. V. C.; Shalgren, C. M. Spatial Patterning of the Notch Ligand Dll4 Controls Endothelial Sprouting *in Vitro*. *Sci. Rep.* **2018**, *8*, 6392.

(57) Lin, S.; Mequanint, K. Bioreactor-Induced Mesenchymal Progenitor Cell Differentiation and Elastic Fiber Assembly in Engineered Vascular Tissues. *Acta Biomater.* **2017**, *59*, 200-209.

(58) Zhang, M.; Desai, T.; Ferrari, M. Proteins and Cells on PEG Immobilized Silicon Surfaces. *Biomaterials* **1998**, *19*, 953-960.

(59) Desai, N. P.; Hubbell, J. A. Solution Technique to Incorporate Polyethylene Oxide and Other Water-Soluble Polymers into Surfaces of Polymeric Biomaterials. *Biomaterials* **1991**, *12*, 144-153.

For Table of Contents Use Only